Acta Cryst E CRYSTALLOGRAPHIC COMMUNICATIONS

ISSN 2056-9890

fac-Acetonitriletricarbonyl(dimethylcarbamodithioato-κ^2S,S')rhenium(I): crystal structure and Hirshfeld surface analysis

Sang Loon Tan,[a] See Mun Lee,[a] Peter J. Heard,[b]‡ Nathan R. Halcovitch[c] and Edward R. T. Tiekink[a]*

[a]Research Centre for Crystalline Materials, School of Science and Technology, Sunway University, 47500 Bandar Sunway, Selangor Darul Ehsan, Malaysia, [b]Office of the Provost, Sunway University, 47500 Bandar Sunway, Selangor Darul Ehsan, Malaysia, and [c]Department of Chemistry, Lancaster University, Lancaster LA1 4YB, UK. *Correspondence e-mail: edwardt@sunway.edu.my

Received 9 January 2017
Accepted 15 January 2017

Edited by W. T. A. Harrison, University of Aberdeen, Scotland

‡ Additional correspondence author, e-mail: pheard@sunway.edu.my.

Keywords: crystal structure; rhenium; dithiocarbamate; carbonyl; Hirshfeld surface analysis.

CCDC reference: 1527565

Supporting information: this article has supporting information at journals.iucr.org/e

The title compound, $[Re(C_3H_6NS_2)(C_2H_3N)(CO)_3]$, features an octahedrally coordinated Re^I atom within a C_3NS_2 donor set defined by three carbonyl ligands in a *facial* arrangement, an acetonitrile N atom and two S atoms derived from a symmetrically coordinating dithiocarbamate ligand. In the crystal, dithiocarbamate-methyl-H$\cdots$O(carbonyl) interactions lead to supramolecular chains along $[36\bar{1}]$; both dithiocarbamate S atoms participate in intramolecular methyl-H$\cdots$S interactions. Further but weaker acetonitrile-C—H$\cdots$O(carbonyl) interactions assemble molecules in the *ab* plane. The nature of the supramolecular assembly was also probed by a Hirshfeld surface analysis. Despite their weak nature, the C—H$\cdots$O contacts are predominant on the Hirshfeld surface and, indeed, on those of related $[Re(CO)_3(C_3H_6NS_2)L]$ structures.

1. Chemical context

The reaction between a secondary amine and carbon disulfide in the presence of an alkali metal hydroxide yields a class of ligands, the dithiocarbamates, $^{(-)}S_2CNRR'$. These ligands have long attracted the attention of coordination chemists owing to their high affinity for heavy-atom centres drawn from transition metals, main group elements as well as lanthanides and actinides. The motivation for their study ranges across various disciplines and in the present time focuses upon their development as drugs (Hogarth, 2012; Bertrand & Casini, 2014), as chelating agents for the removal of toxic levels of metals in bio-remediation, *etc*. (Gallagher & Vo, 2015), as imaging/radio-pharmaceutical agents (Berry *et al.*, 2012) and as synthetic precursors for metal sulfide nanoparticles (Lewis *et al.*, 2015; Knapp & Carmalt, 2016). In terms of crystal engineering endeavours, dithiocarbamates are not nearly as well studied as carboxylates. This partly arises as a result of the greater chelating ability of dithiocarbamate by virtue of the significant contribution of the $^{(2-)}S_2{=}CN^{(+)}RR'$ canonical form to the electronic structure of the anion, *i.e.* with formal negative charges on each of the sulfur atoms. This has the consequence of reducing the Lewis acidity of the metal atom, often precluding additional donor atoms from entering the coordination sphere. Main group element dithiocarbamate compounds are more likely to feature bridging ligands, often through secondary $M\cdots$S interactions which may be mitigated by steric effects associated with the R,R' groups or, in cases of

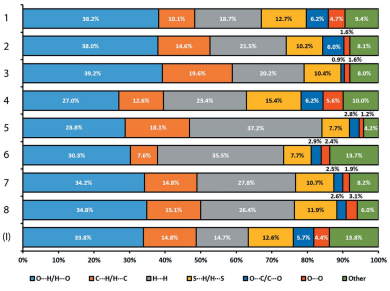

organometallic derivatives, metal-bound substituents (Tiekink, 2006; Tiekink & Zukerman-Schpector, 2010). Another consequence of the tight chelating mode of the dithiocarbamate ligands is the formation of aromatic MS_2C chelate rings that can function as acceptors for C—H$\cdots$ interactions, *i.e.* C—H$\cdots\pi$(chelate) interactions (Tiekink & Zukerman-Schpector, 2011; Jotani *et al.*, 2016). As a result of the above, a very large number of crystal structure determinations have been reported in the literature, with the last systematic reviews published over a decade ago (Heard, 2005; Hogarth, 2005).

Reflecting the wealth of structural information on metal dithiocarbamates, a search of the Cambridge Crystallographic Database (Groom *et al.*, 2016) for rhenium dithiocarbamate structures reveals over 70 'hits'. One structure that attracted the attention of the authors was that of twofold symmetric, binuclear $[(CO)_3Re(S_2CNEt_2)]_2$, whereby each dithiocarbamate ligand is μ_2-tridentate, simultaneously chelating one Re^{I} atom while bridging a second (Flörke, 2014). The unusual feature of the structure is that the dithiocarbamate ligands lie to one side of the molecule and might be described as being *syn*. This arrangement is the same as that found in analogous, isoelectronic Pt^{IV} complexes (Heard *et al.*, 2000), but contradicts the observations seen in the overwhelming majority of the binary dithiocarbamates of the zinc triad elements, a focus of present research, whereby binuclear molecules with equal numbers of chelating and μ_2-tridentate ligands lead to binuclear molecules of the general formula, $\{M(S_2CNRR')_2\}_2$ (Cox & Tiekink, 2009; Tiekink, 2003; Tan *et al.*, 2016; Jotani *et al.*, 2016). This disparity lead to the attempted synthesis of the dimethyldithiocarbamate analogue of $[(CO)_3Re(S_2CNEt_2)]_2$, which when recrystallized from acetonitrile resulted in the isolation of mononuclear $(CO)_3Re(S_2CNMe_2)(N{\equiv}CMe)$, (I). Herein, the molecular and crystal structures of (I) are described along with a detailed analysis of the self-assembly *via* a Hirshfeld surface analysis.

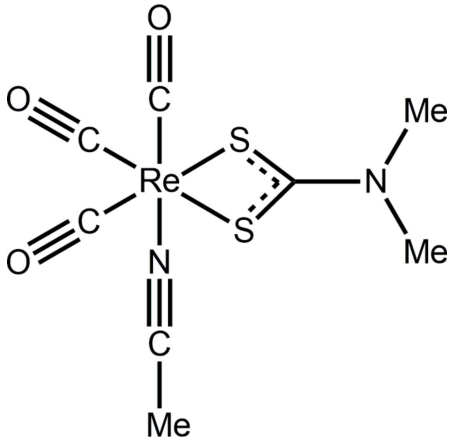

2. Structural commentary

The molecular structure of (I) is shown in Fig. 1 and selected geometric parameters are collected in Table 1. The Re^{I} atom is coordinated by three *facially*-orientated carbonyl ligands, two dithiocarbamate-S atoms and an acetonitrile-N atom. The dithiocarbamate ligand is chelating in a symmetric mode with the difference between the long and short Re—S bond lengths being less than 0.01 Å. This mode of coordination is reflected in the equivalence of the associated C—S bond lengths and a relatively short C1—N1 bond length, Table 1, all pointing to a significant contribution of the $^{(2-)}S_2C{=}N^{(+)}Me_2$ canonical form to the overall electronic structure of the dithiocarbamate ligand. From the geometric data collected in Table 1, there is evidence that the shortest Re—CO bond length is formed by the carbonyl *trans* to the acetonitrile-N atom as opposed to those *trans* to the dithiocarbamate-S atoms. However, the experimental errors do not allow definitive conclusions to be made. This point is discussed further in *Database survey* below.

Table 1
Selected geometric parameters (Å, °).

Re—S1	2.4956 (6)	Re—C5	1.924 (2)
Re—S2	2.5034 (6)	C1—S1	1.722 (2)
Re—N2	2.153 (2)	C1—S2	1.727 (2)
Re—C4	1.909 (3)	C1—N1	1.320 (3)
Re—C6	1.921 (3)		
S1—Re—C5	169.42 (7)	N2—Re—C4	175.53 (9)
S2—Re—C6	168.98 (7)		

3. Supramolecular features

Based on the standard criteria in *PLATON* (Spek, 2009), the most specific directional interaction between molecules in (I) is a dithiocarbamate-methyl-H$\cdots$O(carbonyl) interaction, Table 2. These lead to linear supramolecular chains along [36$\bar{1}$], Fig. 2*a*. Further searching for intermolecular interactions reveals that the two remaining carbonyl-O atoms participate in weak C—H$\cdots$O interactions just below the sum

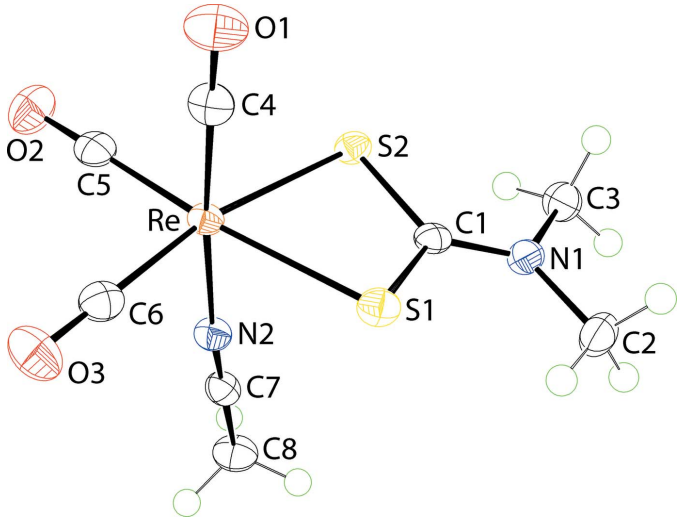

Figure 1
The molecular structure of (I), showing the atom-labelling scheme and displacement ellipsoids at the 70% probability level.

Table 2
Hydrogen-bond geometry (Å, °).

D—H···A	D—H	H···A	D···A	D—H···A
C2—H2B···O1^{i}	0.98	2.59	3.260 (3)	126
C8—H8C···O2^{ii}	0.98	2.69	3.332 (3)	123
C8—H8B···O3^{iii}	0.98	2.69	3.244 (3)	116
C2—H2C···S1	0.98	2.49	3.030 (2)	114
C3—H3A···S2	0.98	2.64	3.035 (2)	105

Symmetry codes: (i) $x+1, y+1, z$; (ii) $x, y+1, z$; (iii) $-x+1, -y+1, -z+2$.

of the van der Waals radii, each with an acetonitrile-C—H atom, Table 2. The combination of these weak interactions leads to supramolecular layers in the *ab* plane, Fig. 2*b*. The two other potentially basic sites, namely the dithiocarbamate-S atoms, form intramolecular interactions with dithiocarbamate-methyl-H atoms, Table 2. The layers stack along the *c* axis as shown in Fig. 2*c*, *i.e.* without directional interactions between them.

4. Hirshfeld surface analysis

The protocols for the Hirshfeld surface analysis were as described recently (Yeo *et al.*, 2016). In general, the Hirshfeld surface of (I) features some close interaction contacts as evidenced from the intense-red spots, Fig. 3*a*, being indicative of d_{norm} contact distances shorter than the sum of van der Waals radii (McKinnon *et al.*, 2007). The combination of the d_i and d_e, in intervals of 0.01 Å, resulted in the sparrow-like two-dimensional fingerprint plot. This has been decomposed into several close contacts as shown in Fig. 3*b*–*f*. Specifically, the intense-red spots resulting from O···H/H···O as well as C···O/O···C contacts give bat- and scarab-shaped fingerprint profiles with corresponding $d_e + d_i$ contact distances tipped at *ca* 2.5 and 3.0 Å, respectively; Fig. 3*b* and *f*. These contact distances are approximately 0.25 Å shorter than the sum of the respective van der Waals radii (Batsanov, 2001) and constitute about 33.8 and 5.7%, respectively, of the overall Hirshfeld surface contacts for the molecule. Other major contacts include C···H/H···C (14.8%), H···H (14.7%) and S···H/H···S (12.6%) which result in the pincer, bust sculpture and pincer forms of the respective decomposed fingerprint plots, despite the fact their contact distance are very close or equivalent to the sum of van der Waals radii with $d_e + d_i$ values of 2.8, 2.4 and 2.9 Å, respectively; see Fig. 3*c*–*e*.

5. Database survey

A series of eight closely related structural analogues with the formula $[Re(CO)_3(S_2CNMe_2)L]$, where L = ammonia (NH_3) (1), pyridine (py) (2), imidazole (Im) (3), pyrazole (pz) (4), triphenylphosphine (PPh_3) (5), 1,3,5-triaza-7-phosphaadamantane (PTA) (6), *t*-butyl isocyanide (tBuNC) (7) and cyclohexyl isocyanide (CyNC) (8) have been reported previously (Herrick *et al.*, 2009). The bond lengths about the Re^{I} atom in 1–8 and (I) are collated in Table 3; the numbering schemes correspond to that shown in Fig. 1. There are a few

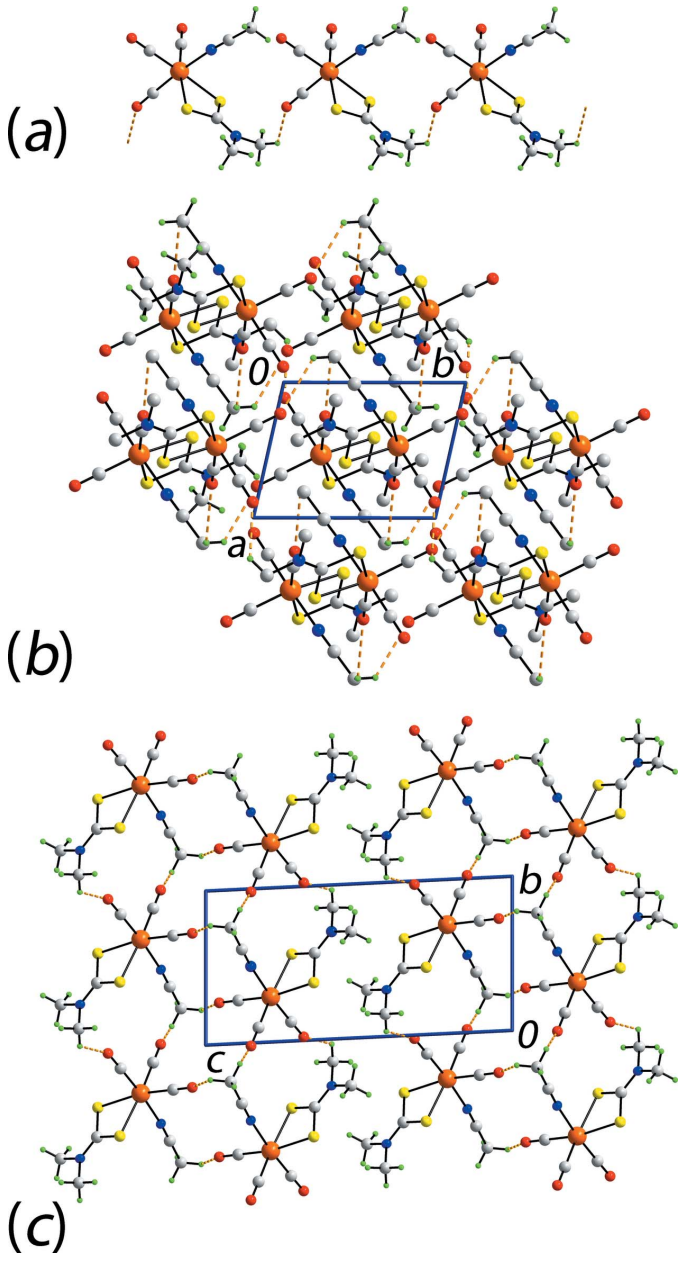

Figure 2
The molecular packing in (I): (*a*) supramolecular chain sustained by methyl-C—H···O(carbonyl) interactions shown as orange dashed lines, (*b*) view of the supramolecular layers in the *ab* plane with non-participating H atoms removed and (*c*) a view of the unit-cell contents in projection down the *a* axis.

general observations that can be noted. Firstly, neither *d*(Re—S1) nor *d*(Re—S2) show major deviations in their respective bond lengths as evidenced from the mean difference of 0.005 Å for each. Despite the small differences, a trend is observed in that *d*(Re—S2) is generally longer than *d*(Re—S1). A consistent pattern is observed in the related *d*(Re—C5), *i.e. trans* to S1, and *d*(Re—C6), *i.e. trans* to S2, bond lengths for which the latter registers an average elongation of 0.005 Å. Secondly, the *d*(Re—*L*) bond lengths are found to consistently increase from C-donor ligands to N-donors, with a

Table 3
Selected bonding parameters (Å) for (I) and literature analogues $[Re(CO)_3(S_2CNMe_2)L]$..

L = ammonia (NH_3) (1), pyridine (py) (2), imidazole (Im) (3), pyrazole (pz) (4), triphenylphosphine (PPh_3) (5), 1,3,5-triaza-7-phosphaadamantane (PTA) (6), *t*-butyl isocyanide (tBuNC) (7) and cyclohexyl isocyanide (CyNC) (8) (Herrick *et al.*, 2009).

L	Re—S1	Re—S2	Re—C	C≡O	Re—C	C≡O	Re—C	C≡O	Re—*L*
			(*trans* to S1)		(*trans* to S2)		(*trans* to *L*)		
(1)	2.497 (2)	2.506 (2)	1.915 (7)	1.164 (8)	1.912 (6)	1.161 (7)	1.916 (7)	1.153 (9)	2.228 (5)
(2)	2.505 (2)	2.498 (1)	1.925 (6)	1.147 (7)	1.929 (5)	1.137 (7)	1.926 (5)	1.141 (7)	2.219 (4)
(3)	2.501 (2)	2.518 (3)	1.937 (7)	1.135 (8)	1.914 (7)	1.157 (9)	1.918 (7)	1.166 (8)	2.189 (6)
(4)	2.489 (4)	2.501 (4)	1.906 (14)	1.147 (17)	1.900 (14)	1.153 (17)	1.912 (13)	1.133 (16)	2.173 (10)
(5)	2.513 (3)	2.506 (3)	1.910 (10)	1.169 (13)	1.895 (10)	1.179 (12)	1.931 (10)	1.152 (12)	2.474 (3)
(6)	2.527 (5)	2.529 (4)	1.925 (15)	1.147 (19)	1.898 (16)	1.160 (20)	1.983 (18)	1.110 (20)	2.437 (5)
(7)	2.512 (3)	2.521 (2)	1.906 (7)	1.176 (9)	1.941 (8)	1.137 (9)	1.955 (8)	1.152 (9)	2.102 (7)
(8)	2.502 (2)	2.512 (2)	1.914 (9)	1.142 (12)	1.908 (10)	1.168 (12)	1.953 (9)	1.125 (11)	2.082 (9)
(I)	2.496 (1)	2.503 (1)	1.924 (2)	1.150 (3)	1.921 (3)	1.145 (3)	1.909 (3)	1.155 (3)	2.153 (2)

ca 0.10 Å or 5% increment, followed by P-donors with about a 0.26 Å or 12% increase, *cf*. the N-donor ligands. However, the observed trend deviates from expectation in that the $d(M-L)$ bond length is anticipated to increase in the order N < C < P-donor type ligand by approximately 2.6 and 27.4%, respectively, based on their calculated covalent bond radii. Further, it is observed that d(Re—C4), *i.e*. with C4 *trans* to *L*, is marginally longer than d(Re—C5) and d(Re—C6) by *ca* 0.01–0.02 Å. Finally, d(C4≡O1) is generally shorter, by about 0.01 Å, *cf*. d(C5≡O2) and d(C6≡O3), *i.e*. with C5 and C6 *trans* to the S1 and S2 atoms, respectively. These observations show the presence of strong π-backbonding prevailing in the C-donor type ligands that result in shorter Re—*L* and longer Re—C4 bonds as well as shorter C4≡O1 bond lengths when

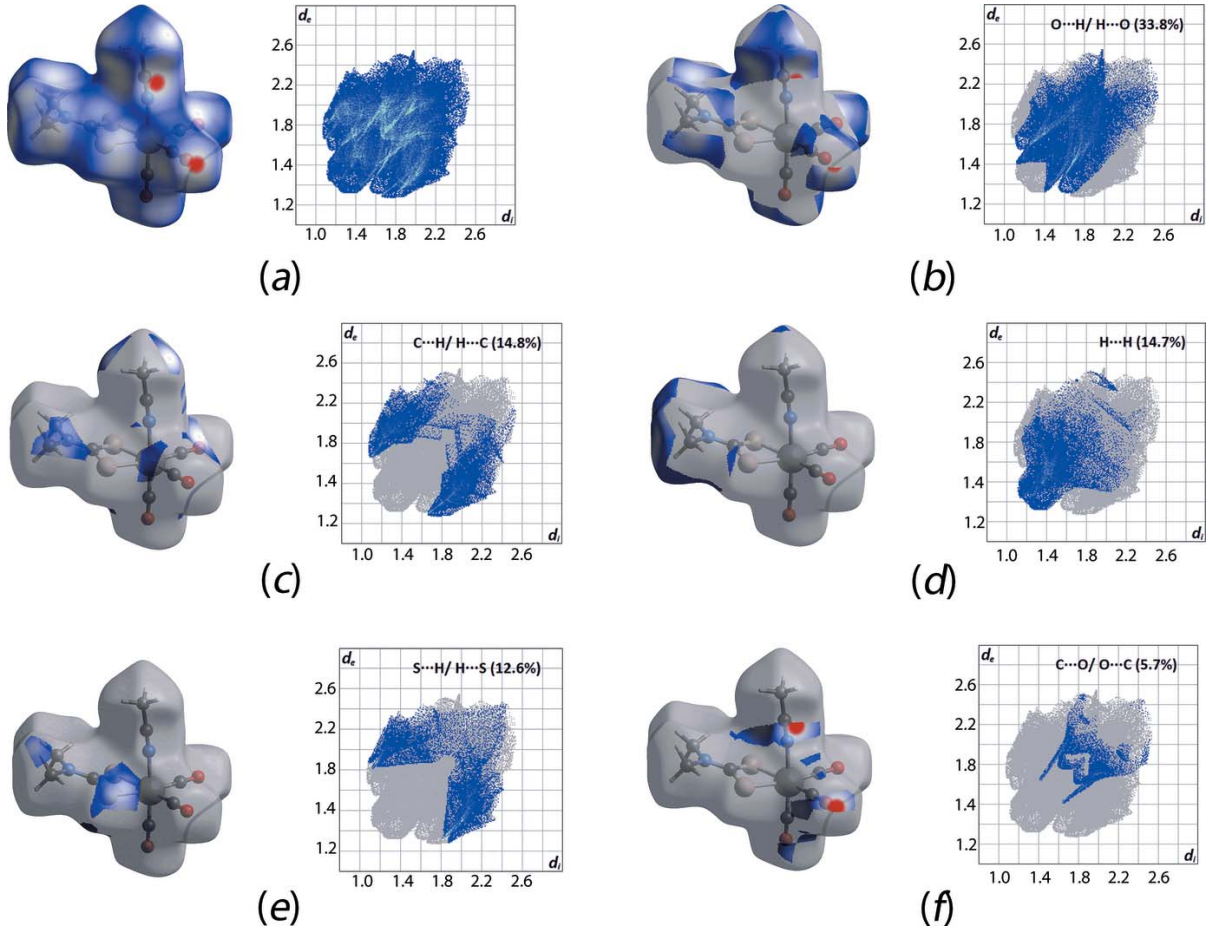

Figure 3
Hirshfeld d_{norm} surface and two-dimensional fingerprint plots for (I): (*a*) full plot, and those decomposed into (*b*) O···H/H···O, (*c*) C···H/H···C, (*d*) H···H, (*e*) S···H/H···S and (*f*) C···O/O···C contacts.

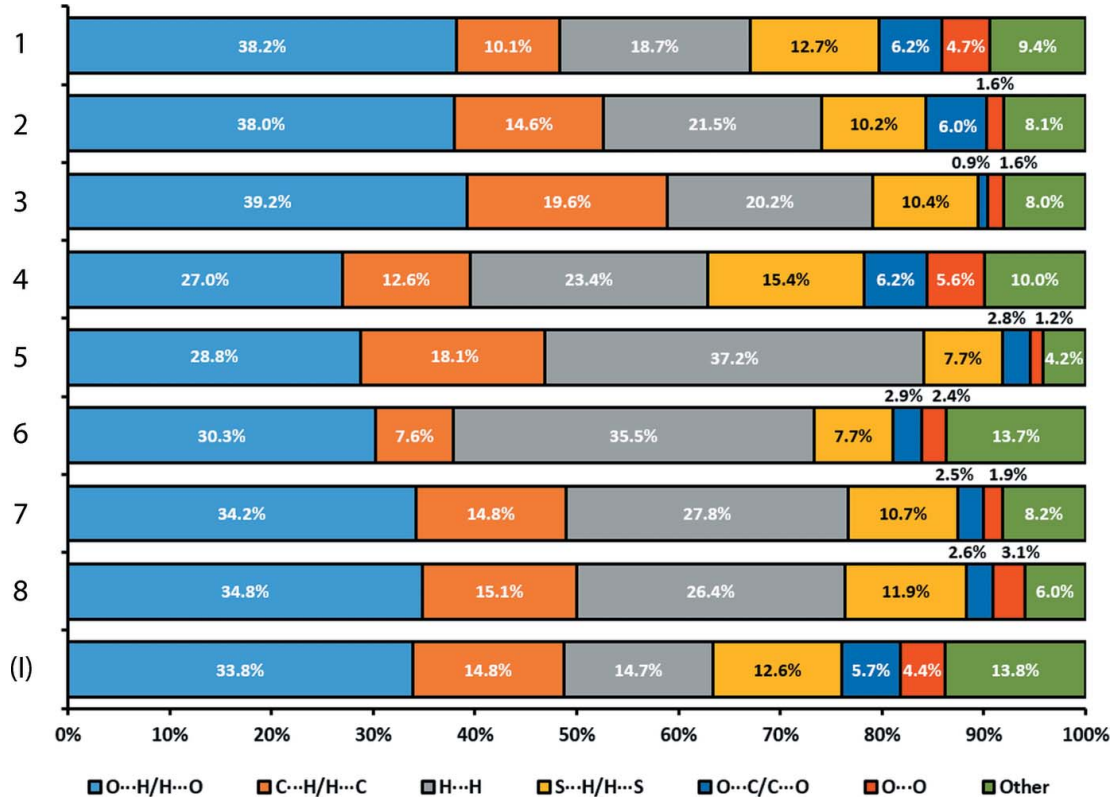

Figure 4
Percentage contributions of the different close contacts to the Hirshfeld surfaces of (I) and 1–8.

compared to the other structural analogues. Further, these trends are clearly reflected in the blue shift of the νCO vibrational band for L = C-type donor ligands, with an average $\Delta\nu = 180$ cm^{-1}, compared with those for N- and P-type donors (Herrick *et al.*, 2009). In the present study, ν(CO) for (I) was observed at 1883 cm^{-1}.

The molecular packing in each of 1–8 was also studied through Hirshfeld surface analysis by calculating the relative composition of each intermolecular close contact present in the structure using *Crystal Explorer* (Wolff *et al.*, 2012); Fig. 4. Generally, the intermolecular close contacts are dominated by O···H/H···O, H···H, followed by either C···H/H···C or S···H/H···S contacts, with the exceptional cases being for 5 and 6, with hydrogen-rich P-donor ligands, for which the dominance is in the order H···H > O···H/H···O > C···H/H···C > S···H/S···H. These results highlight the relative importance of the C—H···O contacts in these structures despite their relatively weak nature.

6. Synthesis and crystallization

All chemicals and solvents were used as purchased without purification, and all reactions were carried out under ambient conditions. The melting point was determined using an Electrothermal digital melting point apparatus and was uncorrected. The IR spectra were obtained on a Perkin Elmer Spectrum 400 FT Mid-IR/Far-IR spectrophotometer from 4000 to 400 cm^{-1} (abbreviations: *vs*, very strong; *s*, strong). ^{1}H NMR spectra were recorded at room temperature in DMSO-d_6 solution on a Bruker AVANCE-400 MHz instrument.

Bromopentacarbonylrhenium(I) (0.25 mmol, 0.102 g) in acetone (10 ml) was added to sodium dimethyldithiocarbamate hydrate (0.25 mmol, 0.036 g) in acetone (10 ml). The resulting mixture was stirred and refluxed for 2 h. The filtrate was evaporated until a precipitate was obtained. The precipitate was recrystallized from its acetonitrile solution. Colourless blocks were obtained from the slow evaporation of the filtrate. Yield: 0.064 g, 60%; M.p. 478–479 K. IR (cm^{-1}): 2009 (*s*), 1883 (*vs*). ^{1}H NMR (in DMSO-d_6): δ 3.21 (*s*, 6H, N–CH$_3$), 2.07 (*s*, 3H, C–CH$_3$).

7. Refinement

Crystal data, data collection and structure refinement details are summarized in Table 4. Carbon-bound H atoms were placed in calculated positions (C—H = 0.98 Å) and were included in the refinement in the riding-model approximation, with U_{iso}(H) set to 1.2U_{eq}(C). The maximum and minimum residual electron density peaks of 0.80 and 1.21 e Å^{-3} were located 0.87 and 0.91 Å, respectively, from the Re atom.

Acknowledgements

We thank Sunway University for support of biological and crystal engineering studies of metal dithiocarbamates.

Table 4
Experimental details.

Crystal data	
Chemical formula	$[Re(C_3H_6NS_2)(C_2H_3N)(CO)_3]$
M_r	431.49
Crystal system, space group	Triclinic, $P\overline{1}$
Temperature (K)	100
a, b, c (Å)	5.7442 (1), 7.5022 (1), 14.6644 (2)
α, β, γ (°)	91.496 (1), 95.517 (1), 102.371 (1)
V (Å^3)	613.71 (2)
Z	2
Radiation type	Mo $K\alpha$
μ (mm^{-1})	10.23
Crystal size (mm)	0.15 × 0.11 × 0.11
Data collection	
Diffractometer	Agilent SuperNova Dual Source diffractometer with an AtlasS2 detector
Absorption correction	Gaussian (*CrysAlis PRO*; Rigaku Oxford Diffraction, 2015)
T_{min}, T_{max}	0.371, 0.503
No. of measured, independent and observed [$I > 2\sigma(I)$] reflections	32146, 3244, 3153
R_{int}	0.033
(sin $\theta/\lambda)_{max}$ (Å^{-1})	0.698
Refinement	
$R[F^2 > 2\sigma(F^2)]$, $wR(F^2)$, S	0.016, 0.035, 1.09
No. of reflections	3244
No. of parameters	148
H-atom treatment	H-atom parameters constrained
$\Delta\rho_{max}$, $\Delta\rho_{min}$ (e Å^{-3})	0.80, −1.21

Computer programs: *CrysAlis PRO* (Rigaku Oxford Diffraction, 2015), *SHELXS97* (Sheldrick, 2008), *SHELXL2014* (Sheldrick, 2015), *ORTEP-3 for Windows* (Farrugia, 2012), *DIAMOND* (Brandenburg, 2006) and *publCIF* (Westrip, 2010).

References

Batsanov, S. S. (2001). *Inorg. Mater.*, **37**, 1031–1046.
Berry, D. J., Torres Martin de Rosales, R., Charoenphun, P. & Blower, P. J. (2012). *Mini Rev. Med. Chem.* **12**, 1174–1183.
Bertrand, B. & Casini, A. (2014). *Dalton Trans.* **43**, 4209–4219.
Brandenburg, K. (2006). *DIAMOND*. Crystal Impact GbR, Bonn, Germany.
Cox, M. J. & Tiekink, E. R. T. (2009). *Z. Kristallogr.* **214**, 184–190.
Farrugia, L. J. (2012). *J. Appl. Cryst.* **45**, 849–854.
Flörke, U. (2014). Private communication (refcode KOGRIJ). CCDC, Cambridge, England.
Gallagher, W. P. & Vo, A. (2015). *Org. Process Res. Dev.* **19**, 1369–1373.
Groom, C. R., Bruno, I. J., Lightfoot, M. P. & Ward, S. C. (2016). *Acta Cryst.* B**72**, 171–179.
Heard, P. J. (2005). *Prog. Inorg. Chem.* **53**, 1–69.
Heard, P. J., Kite, K., Nielsen, J. S. & Tocher, D. A. (2000). *J. Chem. Soc. Dalton Trans.* pp. 1349–1356.
Herrick, R. S., Ziegler, C. J., Sripothongnak, S., Barone, N., Costa, R., Cupelo, W. & Gambella, A. (2009). *J. Organomet. Chem.* **694**, 3929–3934.
Hogarth, G. (2005). *Prog. Inorg. Chem.* **53**, 71–561.
Hogarth, G. (2012). *Mini Rev. Med. Chem.* **12**, 1202–1215.
Jotani, M. M., Tan, Y. S. & Tiekink, E. R. T. (2016). *Z. Kristallogr.* **231**, 403–413.
Knapp, C. E. & Carmalt, C. J. (2016). *Chem. Soc. Rev.* **45**, 1036–1064.
Lewis, E. A., McNaughter, P. D., Yin, Z. J., Chen, Y. Q., Brent, J. R., Saah, S. A., Raftery, J., Awudza, J. A. M., Malik, M. A., O'Brien, P. & Haigh, S. J. (2015). *Chem. Mater.* **27**, 2127–2136.
McKinnon, J. J., Jayatilaka, D. & Spackman, M. A. (2007). *Chem. Commun.* pp. 3814–3816.
Rigaku Oxford Diffraction (2015). *CrysAlis PRO*. Agilent Technologies Inc., Santa Clara, CA, USA.
Sheldrick, G. M. (2008). *Acta Cryst.* A**64**, 112–122.
Sheldrick, G. M. (2015). *Acta Cryst.* C**71**, 3–8.
Spek, A. L. (2009). *Acta Cryst.* D**65**, 148–155.
Tan, Y. S., Halim, S. N. A. & Tiekink, E. R. T. (2016). *Z. Kristallogr.* **231**, 113–126.
Tiekink, E. R. T. (2003). *CrystEngComm*, **5**, 101–113.
Tiekink, E. R. T. (2006). *CrystEngComm*, **8**, 104–118.
Tiekink, E. R. T. & Zukerman-Schpector, J. (2010). *Coord. Chem. Rev.* **254**, 46–76.
Tiekink, E. R. T. & Zukerman-Schpector, J. (2011). *Chem. Commun.* **47**, 6623–6625.
Westrip, S. P. (2010). *J. Appl. Cryst.* **43**, 920–925.
Wolff, S. K., Grimwood, D. J., McKinnon, J. J., Turner, M. J., Jayatilaka, D. & Spackman, M. A. (2012). *Crystal Explorer*. The University of Western Australia.
Yeo, C. I., Tan, S. L. & Tiekink, E. R. T. (2016). *Acta Cryst.* E**72**, 1446–1452.

supporting information

Acta Cryst. (2017). E**73**, 213-218 [https://doi.org/10.1107/S2056989017000755]

fac-Acetonitriletricarbonyl(dimethylcarbamodithioato-κ^2S,S')rhenium(I): crystal structure and Hirshfeld surface analysis

Sang Loon Tan, See Mun Lee, Peter J. Heard, Nathan R. Halcovitch and Edward R. T. Tiekink

Computing details

Data collection: *CrysAlis PRO* (Rigaku Oxford Diffraction, 2015); cell refinement: *CrysAlis PRO* (Rigaku Oxford Diffraction, 2015); data reduction: *CrysAlis PRO* (Rigaku Oxford Diffraction, 2015); program(s) used to solve structure: *SHELXS97* (Sheldrick, 2008); program(s) used to refine structure: *SHELXL2014* (Sheldrick, 2015); molecular graphics: *ORTEP-3 for Windows* (Farrugia, 2012) and *DIAMOND* (Brandenburg, 2006); software used to prepare material for publication: *publCIF* (Westrip, 2010).

fac-Acetonitriletricarbonyl(dimethylcarbamodithioato-κ^2S,S')rhenium(I)

Crystal data

$[Re(C_3H_6NS_2)(C_2H_3N)(CO)_3]$
M_r = 431.49
Triclinic, $P\overline{1}$
a = 5.7442 (1) Å
b = 7.5022 (1) Å
c = 14.6644 (2) Å
α = 91.496 (1)°
β = 95.517 (1)°
γ = 102.371 (1)°
V = 613.71 (2) Å^3
Z = 2
$F(000)$ = 404
D_x = 2.335 Mg m^{-3}
Mo $K\alpha$ radiation, λ = 0.71073 Å
Cell parameters from 22533 reflections
θ = 3.0–29.4°
μ = 10.23 mm^{-1}
T = 100 K
Block, colourless
0.15 × 0.11 × 0.11 mm

Data collection

Agilent SuperNova Dual Source diffractometer with an AtlasS2 detector
Radiation source: micro-focus sealed X-ray tube, SuperNova (Mo) X-ray Source
Mirror monochromator
ω scans
Absorption correction: gaussian (CrysAlis PRO; Rigaku Oxford Diffraction, 2015)
T_{min} = 0.371, T_{max} = 0.503
32146 measured reflections
3244 independent reflections
3153 reflections with $I > 2\sigma(I)$
R_{int} = 0.033
θ_{max} = 29.7°, θ_{min} = 2.8°
h = −7→7
k = −10→10
l = −20→20

Refinement

Refinement on F^2
Least-squares matrix: full
$R[F^2 > 2\sigma(F^2)]$ = 0.016
$wR(F^2)$ = 0.035
S = 1.09
3244 reflections
148 parameters
0 restraints
Hydrogen site location: inferred from neighbouring sites
H-atom parameters constrained

$w = 1/[\sigma^2(F_o^2) + (0.0185P)^2 + 0.3859P]$
where $P = (F_o^2 + 2F_c^2)/3$
$(\Delta/\sigma)_{max} = 0.002$

$\Delta\rho_{max} = 0.80$ e Å^{-3}
$\Delta\rho_{min} = -1.21$ e Å^{-3}

Special details

Geometry. All esds (except the esd in the dihedral angle between two l.s. planes) are estimated using the full covariance matrix. The cell esds are taken into account individually in the estimation of esds in distances, angles and torsion angles; correlations between esds in cell parameters are only used when they are defined by crystal symmetry. An approximate (isotropic) treatment of cell esds is used for estimating esds involving l.s. planes.

Fractional atomic coordinates and isotropic or equivalent isotropic displacement parameters (Å²)

	x	*y*	*z*	U_{iso}*/U_{eq}
Re	0.53372 (2)	0.29366 (2)	0.78801 (2)	0.01195 (4)
S1	0.40857 (10)	0.56377 (8)	0.71937 (4)	0.01596 (12)
S2	0.74400 (10)	0.37175 (8)	0.64780 (4)	0.01389 (11)
O1	0.1152 (3)	0.0231 (3)	0.68068 (14)	0.0259 (4)
O2	0.7673 (3)	−0.0198 (3)	0.85255 (14)	0.0258 (4)
O3	0.2514 (3)	0.2703 (3)	0.95601 (13)	0.0267 (4)
N1	0.6870 (4)	0.6973 (3)	0.58960 (14)	0.0156 (4)
N2	0.8304 (4)	0.4965 (3)	0.85327 (14)	0.0151 (4)
C1	0.6222 (4)	0.5632 (3)	0.64470 (16)	0.0132 (4)
C2	0.5732 (5)	0.8540 (3)	0.58562 (18)	0.0203 (5)
H2A	0.4691	0.8457	0.5280	0.031*
H2B	0.6968	0.9672	0.5888	0.031*
H2C	0.4773	0.8542	0.6374	0.031*
C3	0.8671 (4)	0.6924 (3)	0.52607 (17)	0.0190 (5)
H3A	0.9870	0.6289	0.5534	0.028*
H3B	0.9456	0.8176	0.5137	0.028*
H3C	0.7895	0.6277	0.4685	0.028*
C4	0.2721 (4)	0.1247 (3)	0.72181 (17)	0.0174 (5)
C5	0.6800 (4)	0.0972 (3)	0.82800 (17)	0.0169 (5)
C6	0.3585 (4)	0.2794 (3)	0.89373 (17)	0.0176 (5)
C7	0.9880 (4)	0.6097 (3)	0.88229 (16)	0.0155 (5)
C8	1.1894 (5)	0.7539 (4)	0.91890 (18)	0.0211 (5)
H8A	1.3395	0.7194	0.9075	0.032*
H8B	1.1849	0.7720	0.9851	0.032*
H8C	1.1795	0.8676	0.8888	0.032*

Atomic displacement parameters (Å²)

	U^{11}	U^{22}	U^{33}	U^{12}	U^{13}	U^{23}
Re	0.00998 (5)	0.01241 (5)	0.01239 (5)	0.00051 (4)	0.00076 (3)	−0.00140 (3)
S1	0.0137 (3)	0.0178 (3)	0.0177 (3)	0.0058 (2)	0.0031 (2)	−0.0009 (2)
S2	0.0137 (3)	0.0131 (3)	0.0157 (3)	0.0040 (2)	0.0036 (2)	−0.0003 (2)
O1	0.0174 (9)	0.0261 (10)	0.0292 (10)	−0.0028 (8)	−0.0038 (8)	−0.0079 (8)
O2	0.0241 (10)	0.0208 (9)	0.0329 (11)	0.0067 (8)	−0.0005 (8)	0.0043 (8)
O3	0.0248 (10)	0.0359 (11)	0.0200 (9)	0.0058 (9)	0.0078 (8)	−0.0001 (8)
N1	0.0167 (10)	0.0138 (9)	0.0162 (10)	0.0040 (8)	0.0001 (8)	−0.0002 (8)

N2	0.0146 (10)	0.0153 (10)	0.0152 (10)	0.0027 (8)	0.0023 (8)	−0.0009 (8)
C1	0.0119 (10)	0.0130 (10)	0.0133 (11)	0.0020 (9)	−0.0022 (8)	−0.0030 (8)
C2	0.0227 (12)	0.0163 (11)	0.0232 (13)	0.0073 (10)	0.0004 (10)	0.0038 (10)
C3	0.0194 (12)	0.0175 (12)	0.0190 (12)	0.0008 (10)	0.0037 (10)	0.0020 (10)
C4	0.0142 (11)	0.0192 (12)	0.0186 (12)	0.0025 (10)	0.0037 (9)	−0.0006 (10)
C5	0.0143 (11)	0.0154 (11)	0.0176 (12)	−0.0034 (9)	0.0010 (9)	−0.0027 (9)
C6	0.0164 (11)	0.0170 (11)	0.0189 (12)	0.0043 (10)	−0.0008 (9)	−0.0014 (9)
C7	0.0154 (11)	0.0179 (11)	0.0139 (11)	0.0050 (10)	0.0018 (9)	0.0002 (9)
C8	0.0171 (12)	0.0202 (12)	0.0228 (13)	−0.0012 (10)	−0.0004 (10)	−0.0049 (10)

Geometric parameters (Å, º)

Re—S1	2.4956 (6)	N1—C3	1.463 (3)
Re—S2	2.5034 (6)	N2—C7	1.140 (3)
Re—N2	2.153 (2)	C2—H2A	0.9800
Re—C4	1.909 (3)	C2—H2B	0.9800
Re—C6	1.921 (3)	C2—H2C	0.9800
Re—C5	1.924 (2)	C3—H3A	0.9800
C1—S1	1.722 (2)	C3—H3B	0.9800
C1—S2	1.727 (2)	C3—H3C	0.9800
O1—C4	1.155 (3)	C7—C8	1.453 (3)
O2—C5	1.150 (3)	C8—H8A	0.9800
O3—C6	1.145 (3)	C8—H8B	0.9800
C1—N1	1.320 (3)	C8—H8C	0.9800
N1—C2	1.462 (3)		
S1—Re—C5	169.42 (7)	S1—C1—S2	114.23 (13)
S2—Re—C6	168.98 (7)	N1—C2—H2A	109.5
N2—Re—C4	175.53 (9)	N1—C2—H2B	109.5
C4—Re—C6	89.79 (10)	H2A—C2—H2B	109.5
C4—Re—C5	91.01 (10)	N1—C2—H2C	109.5
C6—Re—C5	91.30 (10)	H2A—C2—H2C	109.5
C6—Re—N2	93.43 (9)	H2B—C2—H2C	109.5
C5—Re—N2	92.03 (9)	N1—C3—H3A	109.5
C4—Re—S1	92.99 (8)	N1—C3—H3B	109.5
C6—Re—S1	98.50 (7)	H3A—C3—H3B	109.5
N2—Re—S1	83.47 (6)	N1—C3—H3C	109.5
C4—Re—S2	93.39 (7)	H3A—C3—H3C	109.5
C5—Re—S2	99.18 (7)	H3B—C3—H3C	109.5
N2—Re—S2	82.89 (5)	O1—C4—Re	179.1 (2)
S1—Re—S2	70.812 (19)	O2—C5—Re	179.5 (2)
C1—S1—Re	87.05 (8)	O3—C6—Re	179.1 (2)
C1—S2—Re	86.69 (8)	N2—C7—C8	179.7 (3)
C1—N1—C2	121.6 (2)	C7—C8—H8A	109.5
C1—N1—C3	121.8 (2)	C7—C8—H8B	109.5
C2—N1—C3	116.5 (2)	H8A—C8—H8B	109.5
C7—N2—Re	175.3 (2)	C7—C8—H8C	109.5
N1—C1—S1	122.93 (18)	H8A—C8—H8C	109.5

N1—C1—S2	122.84 (18)	H8B—C8—H8C	109.5
C2—N1—C1—S1	−2.5 (3)	Re—S1—C1—N1	−170.0 (2)
C3—N1—C1—S1	−179.31 (18)	Re—S1—C1—S2	10.24 (11)
C2—N1—C1—S2	177.28 (18)	Re—S2—C1—N1	170.0 (2)
C3—N1—C1—S2	0.5 (3)	Re—S2—C1—S1	−10.21 (11)

Hydrogen-bond geometry (Å, º)

D—H···*A*	*D*—H	H···*A*	*D*···*A*	*D*—H···*A*
C2—H2*B*···O1^{i}	0.98	2.59	3.260 (3)	126
C8—H8*C*···O2^{ii}	0.98	2.69	3.332 (3)	123
C8—H8*B*···O3^{iii}	0.98	2.69	3.244 (3)	116
C2—H2*C*···S1	0.98	2.49	3.030 (2)	114
C3—H3*A*···S2	0.98	2.64	3.035 (2)	105

Symmetry codes: (i) *x*+1, *y*+1, *z*; (ii) *x*, *y*+1, *z*; (iii) −*x*+1, −*y*+1, −*z*+2.